



Synergistic Impact of Biochar Nanorods on the Performance of Polyacrylamide Matrix: UV-assisted Degradation of Phenol and Biological Activity



Rehab M. Abo-Ouf^a, Ahmed F. Ghanem^{b,*}, Ahmed A. Youssef^{b,*},
Dalia M. Ayad^a, Magdy Y. Abdelaal^a

^a Mansoura University, Mansoura 35516, Egypt

^b Packaging Materials Department, Chemical Industries Research Institute,
National Research Centre, 33 El Behooth St., Dokki, Giza, Egypt

Abstract

Phenol is present on the top list of toxic pollutants. Enormous researches discussed phenol removal from the wastewater with hydrogels incorporated with biochar utilizing adsorption technique. However, no available information has been recorded investigating the ability of biochar-based nanocomposite hydrogel to degrade phenol under light irradiation as well as studying its biological activity. Accordingly, this work aims at preparation of the biochar nanorods (BNRs) from the rice husk as a precursor. Then, BNRs were included in the polyacrylamide matrix (PAH) via in-situ polymerization with 0.15 wt.%. The obtained BNRs, PAH, and their nanocomposite hydrogel (PABN) were well-characterized. Scanning electron microscope (SEM), transmission electron microscope, X-ray diffraction (XRD), and Fourier transfer infrared (FTIR) confirmed the successful preparation of biochar rods in the nano scale and its effective inclusion in the PAH matrix. Also, thermal gravimetric analysis (TGA) exhibited improvement in the thermal stability of PABN by ~ 10 %. Moreover, surface texture, in terms of surface area and pore size/radius, and the energy band gap were determined with the N₂ adsorption-desorption and the spectroscopic analysis, respectively, for the obtained hydrogels. The removal of phenol was implemented under UV luminance and in the dark. Despite, PABN has a lower surface area and a larger band gap, it exhibited 90 % removal of phenol under the irradiation conditions and 65 % in the dark, higher than the pristine matrix, confirming the impact of photocatalysis. Antimicrobial evaluation proved the biocidal potential of PABN against Gram-positive and Gram-negative bacteria in addition to yeast. It could be claimed that the obtained nanocomposite hydrogel-based biochar and polyacrylamide paves the way towards a next generation of highly effective photocatalysts and bactericidal agent for water treatment applications with economic and environmental impacts.

Keywords: Polyacrylamide; Biochar; Nanocomposites; Water treatment; Photocatalysis; Phenol degradation

1. Introduction

Phenols and their synthetic derivatives have a wide range of industrial applications such as plastics, resins, pharmaceutical products, pesticides, and oil refinery[1-4]. However, they are listed as toxic organic pollutants according to the Document of United State Environmental Protection Agency (USEPA) [5]. Phenolic compounds have serious effects on the aquatic systems and the human' health such as liver, kidney, and nervous diseases due to the

continuous disposal in the wastewater [6]. Nevertheless, the accepted limit of phenol is 1 mg/L in the wastewater [7]. Therefore, the current research focuses to develop powerful techniques and high-performance materials that have the ability to remove these pollutants from the wastewater. For instance, adsorption, chemical oxidation, liquid-liquid extraction, and biological treatment are the most common techniques used for decontamination of water from the organic poisons [8-12]. These systems have pros, such as the high efficiency and the durability, and cons such as the cost, the complex

*Corresponding author e-mail: a7mdghanem@gmail.com (Ahmed Ghanem)

Receive Date: 19 July 2023 Revise Date: 27 August 2023 Accept Date: 31 August 2023

DOI: 10.21608/EJCHEM.2023.223928.8282

©2024 National Information and Documentation Center (NIDOC)

operation, and the poisonous residues [13]. Particularly, photocatalysis deems a promising alternative in the recent years in the removal of organic pollutants thanks to its outstanding features. It has economic impacts since UV and visible light radiations are used. Also, photocatalysis considers an efficient process since no waste is obtained, due to the complete mineralization of the polluted water, and hence environmental impacts [14].

Among the frequently used materials in the water treatment applications, hydrogels are cross-linked networks of hydrophilic polymers with a high swelling capacity in water [15]. Hydrogels showed high efficiency in removing of the water contaminants such as dyes, heavy metals, and organic pollutants [16]. For name but a few, poly (acrylic acid -co- vinyl phosphonic acid) hydrogel cross-linked with N -maleyl chitosan eliminated crystal violet and methylene blue dyes with the adsorption capacity of 64.56 mg/g and 66.89 mg/g, respectively [17]. In another study, grafted cellulose hydrogel was found as a promising adsorbent for phenols with the maximum adsorption capacity of 80.71 mg/g, which is ~ 3 times greater than the traditional carbon-based materials [18]. Dutra *et al.* proved that polyacrylamide/ starch hybrid hydrogels could adsorb phenol from the wastewater with the maximum adsorption capacity of 21 mg/g [19]. On the other hand, hydrogels are considered as proper substrates to host the nanomaterials within their matrices. These hybrid structures display synergistic effects when mixed with the contaminants and hence improve the efficiency of the removal process [20]. For instance, collagen-based hydrogel nanocomposites showed the maximum adsorption capacity of cationic dye more than 90% [21]. Wang and his colleagues have prepared nanocomposite hydrogels based on hydroxypropyl cellulose and graphene oxide [22]. Their results emphasized the strong affinity of these hydrogels towards phenol even after six adsorption-desorption cycles. A recent interesting study has been published studying the removal of carcinogenic dyes using composite hydrogel based on bacterial cellulose incorporated with zeolite particles [23].

Indeed, biochar (BR) is one of carbonaceous materials that can be obtained in the nanoscale [24]. BR have unique characteristics such as high surface area, high exchange capacity, inexpensive material, and low bulk density [25]. Biochar can be obtained from the biomass residues via pyrolysis at the optimized temperatures [26]. In particular, biochar has a strong applicability in the water treatment due to its high affinity to adsorb the toxic compounds on its surface and cost-effective adsorbent [27]. Therefore, several articles incorporated biochar,

produced from different sources, in the hydrogel matrices (hydrogel-biochar composite) in order to improve the performance of the neat polymers towards the removal of organic or even inorganic pollutants. For illustration, a composite hydrogel based on poly acrylamide and rice husk biochar-hydrogel exhibited a maximum sorption capacity for arsenic of 28.32 mg/g [28]. Another hydrogel included rice husk biochar displayed a maximum sorption capacity for zinc 35.75 mg/g [29]. Phenol was effectively removed by several composite hydrogels contain biochar derived from various resources as follows: - (I) Composite hydrogel based on polyacrylamide and palm kernel shell biochar showed a maximum sorption capacity of 19.05 mg/g [30]. (II) Karakayun and his colleagues developed three composite hydrogels [31]. Each hydrogel was incorporated with biochar from different sources. The results presented a diversity in the adsorption capacities by changing the biochar source. Hydrogels contain chicken biochar, wood biochar, and tire biochar exhibited phenol adsorption per unit mass of 29.77 mg/g, 30.68 mg/g, and 17.29 mg/g, respectively. (II) Polyacrylamide / rice husk biochar composite hydrogel was used to remove phenol and p-nitro phenol by adsorption technique [32]. In their study, people found that the highest removal of phenol and p-nitrophenol, of concentrations 50 mg/L, was 82.2% and 84.6%, respectively, after 10 days.

For the best of our knowledge, the photo degradation of phenol was not discussed before over polyacrylamide / rice husk biochar nanocomposite hydrogel. All the previous studies used hydrogels-based biochar as adsorbents rather than as photocatalysts. Accordingly, in the present study, biochar was successfully prepared in the nano scale via pyrolysis of rice husk residues. Then, the obtained nanorods were incorporated during the polymerization of acrylamide in order to eventually obtain polyacrylamide / biochar nanocomposite hydrogel. Various physical characterizations were used to investigate the produced samples. Particularly, the prepared hydrogels were studied as photocatalysts irradiated under UV in the synthetic phenolic water and the removal was detected over the time. Moreover, literatures are lack in information about the biocidal potential for this type of hybrids which intensively investigated during this study.

2. Experimental

2.1 Materials

Acrylamide (AAM, 99%), as a commercial monomer, was purchased from ALPHA CHEMIKA, India. N, N' methylene Bis acrylamide (NNMBA), as a cross-linker, was bought from Sisco Research Laboratories Pvt. Ltd. (SRL), India. Potassium per sulphate (K₂S₂O₈, 99.99 %), as an initiator, was provided from Sigma-Aldrich, St. Louis, USA. Rice husk was collected from the Egyptian environment, well-washed with the deionized water, and dried in the oven at 105 °C overnight in order to get rid of the moisture content.

2.2 Preparation of Polyacrylamide Hydrogel (PAH)

Poly acrylamide hydrogel was prepared by dissolving 12 g of acrylamide monomer in 100 mL distilled water. Then, the solution of NNMBA (0.2 g in 2 mL) was added carefully to the previous solution and the reaction mixture was left under vigorous stirring in a water bath for 20 min. at 60 °C. After that, potassium per sulfate (0.2 g in 2 mL) was inserted drop-wise in order to initiate the polymerization reaction. Two hours later, the reaction was stopped and the produced hydrogel was washed several times by decantation and finally dried in the vacuum oven at 60 °C overnight (Scheme 1).

2.3 Synthesis of Biochar Nanorods (BNR)

Utilizing a pilot-scale electric pyrolyzer with a maximum batch processing capacity 10 kg, biochar was obtained. In the typical procedure, the rice husk, as a raw material, was fully loaded in the combustion chamber and the air was swapped out with the nitrogen gas. Then, the carbonization was carried out at 420 °C (3.5 °C/ min.) for an hour (Scheme 1). After that, the sample was cooled to the ambient temperature followed by collecting and packaging in a stainless-steel container to avoid the oxygen exposure.

2.4 Preparation of Polyacrylamide / Biochar Nanocomposite Hydrogel (PABN).

The polyacrylamide / biochar-based nano composite hydrogel was obtained through in-situ polymerization process. Following the same procedure mentioned in section 2.2, acrylamide monomer (12 g) was dissolved in 100 mL distilled water and then, various amounts of the prepared biochar (0.05, 0.1, and 0.15 wt.%) were wisely added. The reaction mixture was sonicated for 60 min. and left under a vigorous stirring for a further 3 hrs. till attaining a homogeneous dispersion. Then, the solution of

NNMBA (0.2 g in 2 mL) was added carefully to the prepared suspension followed by a vigorous stirring in a water bath for 20 min. at 60 °C. After that, potassium per sulfate (0.2 g in 2 mL) was inserted drop-wise and the reaction was continued for 2 hrs. Finally, the produced nanocomposite hydrogel was well-washed and dried in the vacuum oven at 60 °C overnight (Scheme 1).

2.5 Techniques

2.5.1 Morphology

Scanning electron microscope images were captured for the prepared samples by JEOL-SEM with an acceleration voltage of 80 kV. Particularly, hydrogel samples were scanned after drying. Moreover, transmission electron microscope provided an image for the obtained biochar nanorods as an additional confirmation for its morphology.

2.5.2 Structural analysis

Fourier transform infrared (Perkin Elmer, USA) was used in order to investigate the functional groups propagated on the surface of prepared powders and illustrate the nature of interaction within the nanocomposite hydrogel. On the other hand, X-ray diffraction spectrum was displayed by Bruker diffractometer (Bruker D 8 advance target) for the biochar sample to explore its crystallography. The analysis was operated with a radiation source (CuK α), a secondly monochromator ($k = 1.5405 \text{ \AA}$, at 40 kV, and 40 mA), and a scanning rate (0.2 min^{-1}).

2.5.3 Thermal analysis

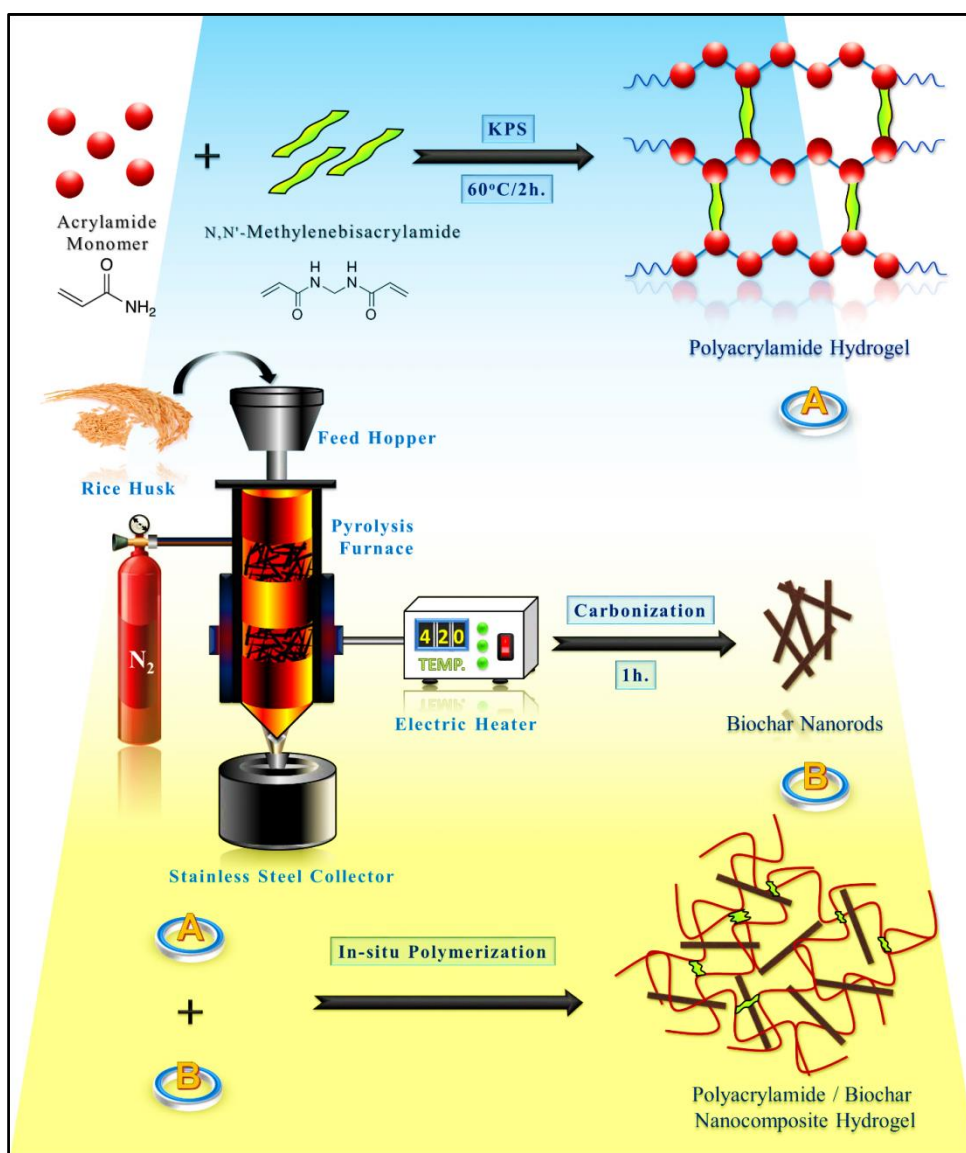
Thermal degradation behavior for the prepared hydrogels were evaluated using Simultaneous DSC-TGA instrument (SDT Q600, USA).

2.5.4 Surface Texture

he surface properties were investigated for the prepared hydrogels with Quantochrome Nova-Touch 4LX automated gas-sorption apparatus (USA).

2.5.5 Band gap

The band gap was measured for the prepared hydrogels with UV-vis spectrophotometer (T80 + UV-vis, PG Instruments Ltd.) on the reflection mood of analysis. The energy band gap values were calculated using Kubelka-Munk function (KM-Function) [33].



Scheme 1: Representation steps for the preparation of polyacrylamide, biochar nanorods, and their nanocomposite hydrogel

2.5.6 Photocatalysis evaluation

A stock of phenol solution (600 mg/L) was prepared. One gram of the prepared hydrogels was mixed separately with 500 mL taken from the as prepared phenol stock. The mixture was irradiated under UV lamp ($\lambda=368$ nm). Over four hours of treatment, a sample was withdrawn each 20 min. and the organic content was evaluated using chemical oxygen demand (COD) in mg/L. The previous steps were done in dark in order to confirm the photocatalytic activity for the prepared catalysts.

2.5.7 Biological evaluation

The antimicrobial effect of the prepared nanocomposite hydrogel compared to the pristine materials was investigated against Gram-positive bacteria (*Staphylococcus aureus* and *Bacillus cereus*), Gram-negative bacteria (*Escherichia coli* and *Pseudomonas aeruginosa*), and yeast (*Candida albican*).

In the typical procedure [34], 1 mg of the sample was incubated under shaking with (50 μ L) of bacterial suspension inoculated to 5 mL of nutrient broth in a sterilized test tube at 37 °C for 24 h. The biocidal potential of the sample was determined by measuring the optical density (OD) with UV-vis spectro-photometer at a fixed wavelength (600 nm).

On the other hand, colonies forming unit (CFU) method was also performed in order to confirm the biological strength of the prepared materials.

3. Results and Discussion

3.1 Microscopic Analysis

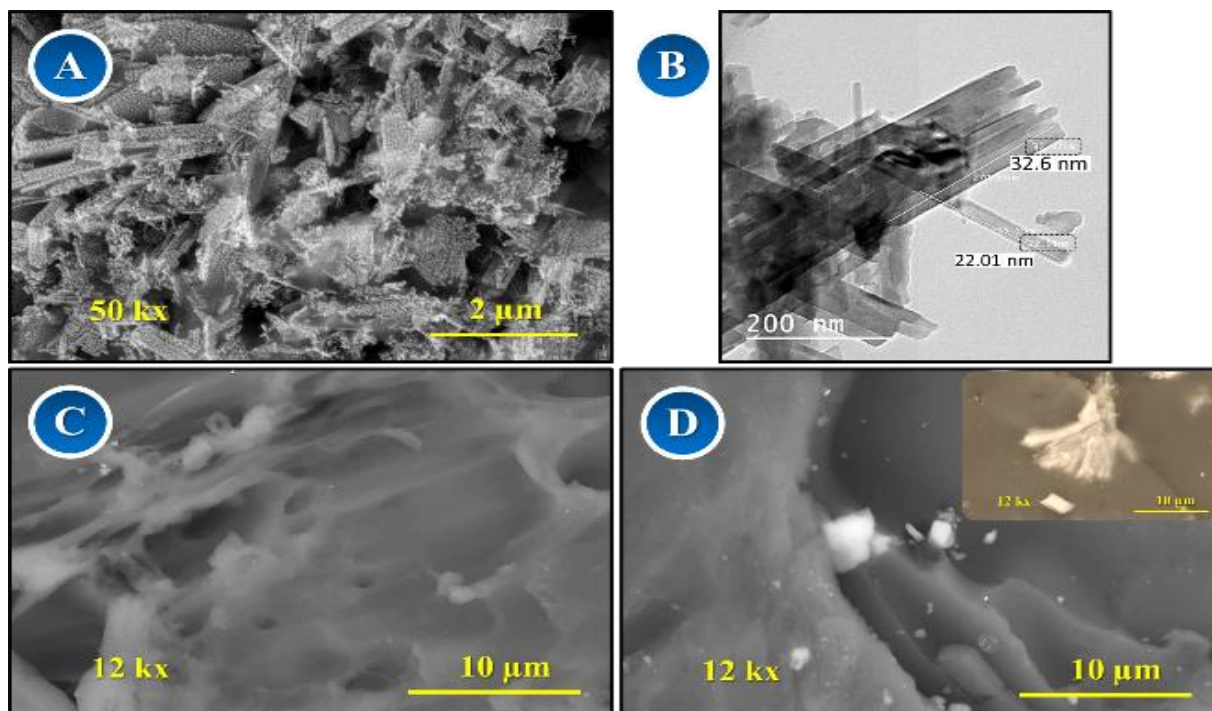


Figure 1: Scanning electron microscope images of biochar nanorods (A), polyacrylamide hydrogel (C), and their nanocomposite (D). Inset represents a different scenery of polyacrylamide/biochar nanocomposite hydrogel. Image (B) is the transmission electron microscope micrograph of the obtained biochar nanorods.

SEM micrographs of the obtained biochar nanorods, polyacrylamide hydrogel, and their nanocomposites are depicted in Fig. 1(A, C-D). Particularly, Fig. 1(A-B) confirmed the rod like structure of the prepared biochar. Obviously, different sizes of the nano rods are composed in separate and aggregates bundles morphology. Indeed, the morphology of the produced biochar strictly depends on the pyrolysis conditions even the source is the same [35, 36]. Fig. 1(C) displays the microstructure of the synthesized hydrogel sample in the dried solid state. Significantly, the sample has heterogeneous porosity as the pores have different sizes. This morphology resembles the previously reported by Kim et al. [37]. Incorporation of the biochar nanorods into PAH matrix causes filling of its micro pores without affecting the polymer structure, Fig. (D). Also, some nanorods agglomerations can be noticed, Fig. (D, inset image).

3.2 Fourier Transform Infrared (FTIR)

Surface functional groups present on the backbone of the prepared samples were investigated with FT-IR measurement in the mid infrared region between

4000 and 400 cm^{-1} , Fig. 2. PAH spectrum shows a broad band with a small shoulder at 3455 and 3230 cm^{-1} attributed to symmetric and asymmetric stretching of $-\text{NH}_2$ groups, respectively [38]. Further bands pronounced at ~ 2928 , 1640, 1618, 1412, and 1120 cm^{-1} assigned to $-\text{CH}$ aliphatic, $-\text{C}=\text{O}$, $-\text{N}-\text{H}$, $-\text{C}-\text{N}$, and $\text{C}-\text{C}$ groups, respectively [38]. However, BNR displays a relatively wide band at $\sim 3430\text{ cm}^{-1}$ corresponds to the vibration of $-\text{OH}$ groups. Other peaks observed at 1730 and 1625 cm^{-1} are referred to the $\text{C}=\text{O}$ and $\text{C}=\text{C}$ stretching vibrations, respectively [39]. However, these peaks are overlapped and the peak corresponding to carbonyl group appeared with a low intensity. Some weak bands were also detected, between 1000 and 1400 cm^{-1} , corresponding to the OH bending and $\text{C}-\text{O}$ stretching vibrations [39, 40]. Indeed, the presence of various surface functional groups on the biochar backbone enhanced the interaction with the polymeric matrix. Therefore, incorporation of biochar in polyacrylamide matrix, PABN, showed broadening and overlapping of their peaks indicating the strong physical interaction within the nanocomposite matrix i.e. the peak assigned at $\sim 3430\text{ cm}^{-1}$ was shifted to a lower wave number and became broader which might be

attributed to the possible hydrogen bonding between the oxygenated functional groups like hydroxyl groups and carbonyl of biochar and amide groups of

PAH causing shifting and overlapping of their peaks [41], Fig. 2.

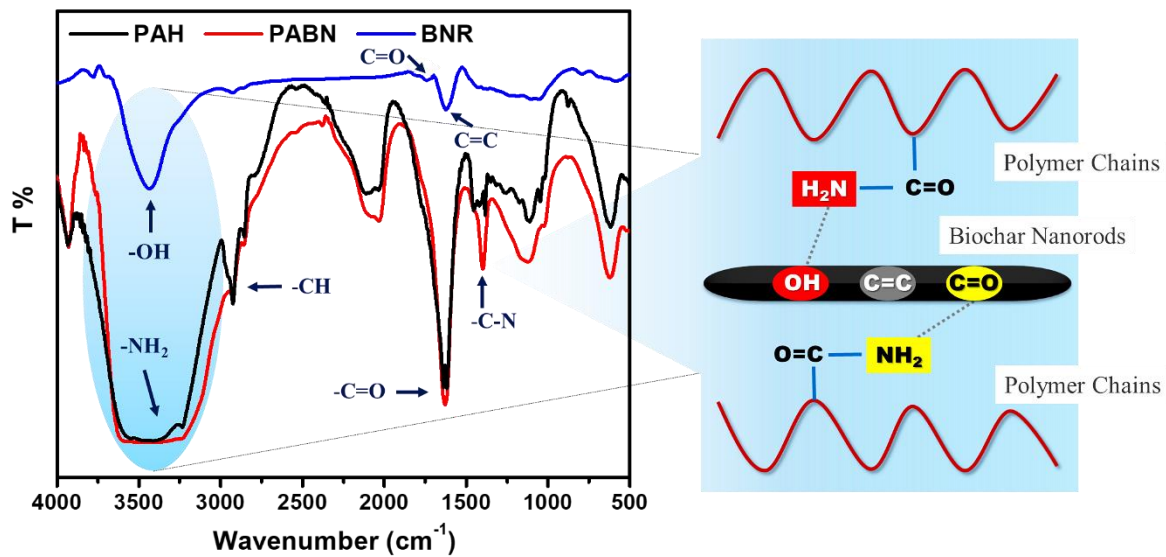


Figure 2: [Left] FTIR spectra of the prepared biochar, pure polyacrylamide hydrogel, and their nanocomposite. [Right] Schematic representation for the interaction within the nanocomposite matrix

3.3 X-ray Diffraction (XRD)

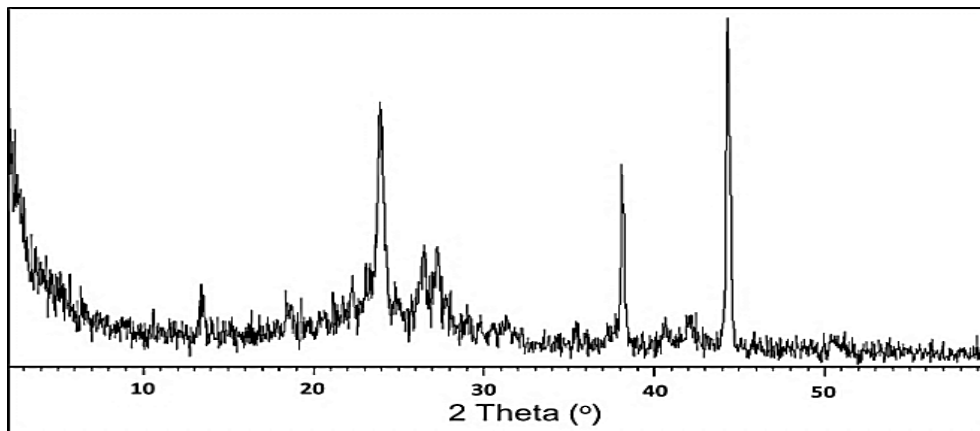


Figure 3: X-ray diffraction spectrum of the prepared biochar.

As shown in Fig. 3, strong X-ray diffraction patterns emerged at $2\theta = 25^\circ$ and $2\theta = 45^\circ$ which indicate the existence of the graphitic structure in the prepared sample. The sharpness of these peaks

emphasizes the successful decomposition of cellulose upon heating producing biochar as well as the smaller crystallite size. Some other observed peaks might be related to the metallic residues. These results are in accordance with the state of the art [40, 42, 43].

3.4 Thermal Analysis

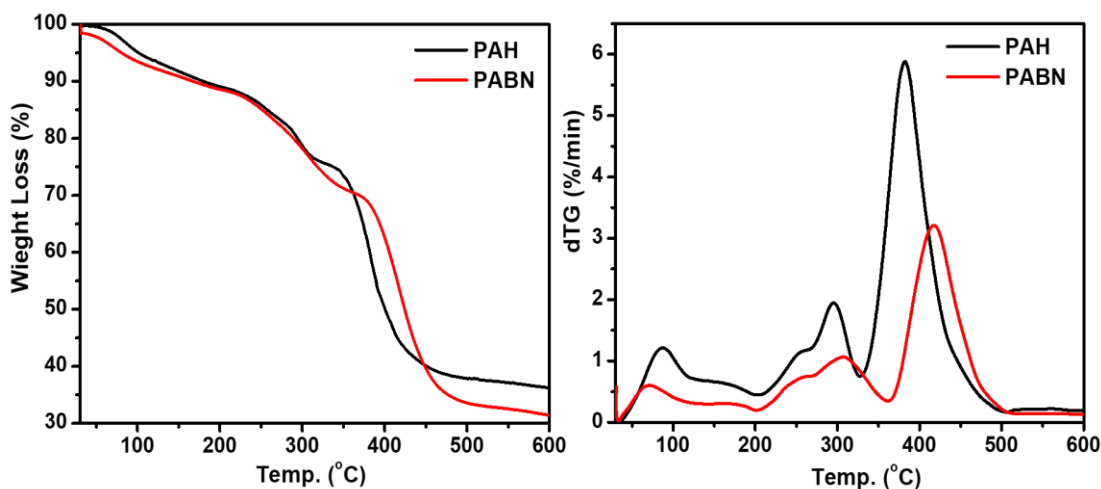


Figure 4: TGA and DTG of the prepared biochar, pure polyacrylamide hydrogel, and their nanocomposite.

The effect of biochar on the thermal properties of PAH was studied using TGA and DTG, Fig. 4. As shown, the prepared samples exhibited a weight loss in different degradation steps.

Both hydrogels lost 10 wt.% at ~ 170 °C due to the removal of water contents. However, PAH started the second degradation stage in the range between 170 and 310°C as it lost ~ 25 wt. % of its weight at the end of this step. The DTG peak was also observed at ~ 295°C. This might be attributed to the amide groups decomposition releasing the ammonia gas and the crosslinker used [44].

After that, PAH started a further weight loss up to 60% in the range between 310 and 450°C, DTG peak is at ~ 380°C, which corresponds to the decomposition of the remaining backbone [45]. These findings are in accordance with the state of art [44]. While incorporation of biochar inside the PAH matrix, the thermal degradation behavior was changed as the hydrogel tended to be maintained at higher temperatures and the degradation point was significantly shifted to a greater value. Obviously, the second step of PABN ends with ~ 30 % weight loss at ~ 360 °C. Meanwhile, the third degradation step terminates with ~ 65 % weight loss at 500 °C. Moreover, the degradation temperature was shifted

by ~ 40 degrees, from 380 to 420 °C. No doubt, inclusion of biochar nanorods in the polyacrylamide matrix improves its thermal stability. These results emphasized also the strong interaction within the obtained nanocomposite. It is worth to mention that biochar is used as a filler for polymer matrices as it enhances their thermal and mechanical properties [46].

3.5 Texture Analysis

Figure 6 represented the isotherms of the N₂ adsorption / desorption for the prepared hydrogels. Obviously, PAH and PABN display IV type of isotherm and H3 type of hysteresis loop. This is accompanied by a higher steep in the former sample than the latter one between the relative pressures of 0.8-0.85. This might be accredited to the capillary condensation phenomena occurs in the pores of the tested adsorbate. Obviously, from Fig. 6 and Table 1, compared with the nanocomposite hydrogel (PABN), pristine polymer (PAH) showed significant high pore diameter and mesoporous volume, high surface areas of BET, Langmuir, and BJH, and high total pore volume with high correlation coefficient ($R^2 > 0.96$). Despite biochar can be used as a mesoporous agent [47], it causes blocking for the surface pores of the hydrogel when incorporated within the polymeric matrix. This result is in accordance with the SEM images. However, these findings did not negatively affect its performance on the phenol removal as will be discussed later on.

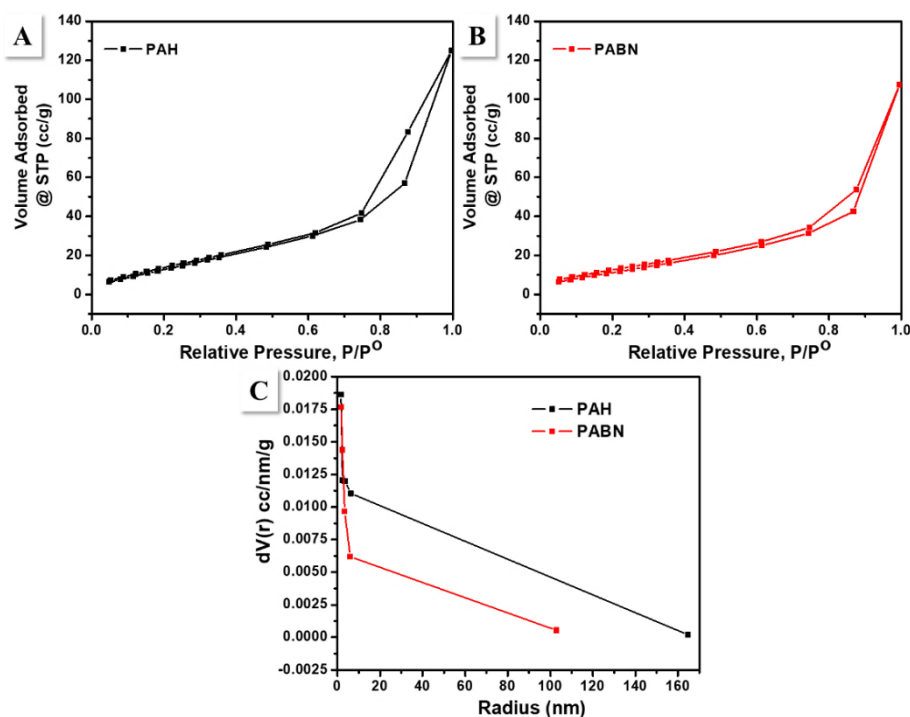


Figure 6: [A- B] N₂ adsorption-desorption isotherms of pure polyacrylamide hydrogel (PAH) and its biochar nanocomposite (PABN), respectively. [C] Their corresponding pore size distribution by BJH- method.

Table 1: Textural properties of the polyacrylamide hydrogel (PAH), and its biochar nanocomposite (PABN).

Textural Parameters	PAH	PABN
Multipoint BET surface area (m ² /g)	59.76	48.51
Correlation coefficient (R ²)	0.967	0.975
Langmuir method (m ² /g)	118.012	89.666
Adsorption BJH surface area (m ² /g)	48.623	37.123
Adsorption BJH cumulative micropore volume (cc/g)	0.188	0.159
Pore radius BJH adsorption (nm)	1.703	1.703
Total pore volume (cc/g)	0.193	0.166
Average pore radius (nm)	6.487	6.875
Average Particle radius (nm)	2.281	2.811

One of the main factors that may contribute in the explanation of phenol degradation over the prepared hydrogels under the UV irradiation is the band gap. Some polymers and other carbonaceous materials have band gap values [48-53] i.e., they are semiconductors. This means that, while irradiation of such substances under UV, they absorb the photon energy of a specific wavelength and jump from the valance band to the conduction band causing an oscillation [54]. Therefore, the optical band gap energy of the polyacrylamide and its nanocomposite

was calculated according to Kubelka–Munk function [54] that applied on the diffuse reflectance spectra results, Fig 7[A]. Particularly, the plots of Kubelka in Fig. 7[B-C] indicate the following: (I) The pristine polyacrylamide has a band gap value of ~ 4.6 eV which is close enough to the previously reported value by Rawat et. al [50]. (II) While inclusion of biochar in the PAH, the band gap showed a drastic increment by ~ 1.8 eV i.e., PABN recorded a band gap of 6.37 eV. This means that biochar acted as an insulating barrier as the band gap of PAH increased.

Indeed, it was expected that biochar would decrease the band gap as it is among conductive carbonaceous materials [55]. Unfortunately, the opposite was totally occurred. This might be attributed to the presence of structure defects in the carbon structure and the conditions of pyrolysis as the conductivity of biochar increases with temperature [56]. In addition, the surface functional groups on the biochar (c.f. Fig. 2) that are tightly bonded with the polymer backbone. No doubt, this might decrease the degree of disorder within the composite matrix which is responsible for the decline of the localized energy

level concentration, hence, reflects an increase in the optical band gap [48]. Nevertheless, in the present study, this might be favorable since increasing of band gap usually leads to decrease the electron-hole recombination and increase the life time of the excited electrons which strongly impact on the photocatalytic performance of the photocatalyst as will be discussed later on. Ghanem et. al stated that addition of ZnO nanorods to the polyester matrix increased the band gap which induced the photocatalytic degradation of phenolic compounds [57].

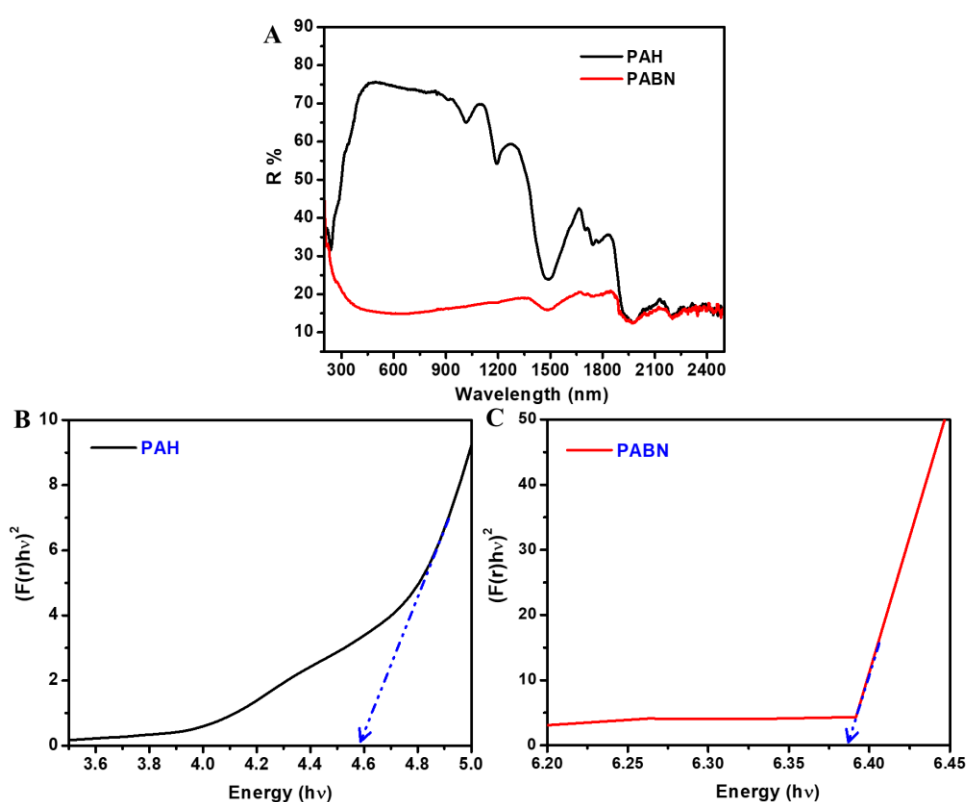


Figure 7: [A] DRS spectra and [B-C] Band gap of polyacrylamide hydrogel (PAH) and its biochar nanocomposite (PABN), respectively.

3.6 Photocatalytic Degradation of Phenol

The photocatalytic activity of PAH and its nanocomposite hydrogel was investigated for the first time in this work. The prepared hydrogels were irradiated under UV lamp and the removal percentage of phenol from the synthetic wastewater was calculated by measuring COD of the water over the reaction time. After the first run, the hydrogels were re-evaluated once again to investigate their durability in the second run. Besides, the first run was repeated

but in the dark to confirm the impact of photocatalysis process over the obtained hydrogels. The effect of UV lamp in absence of photocatalysts was also studied.

From Fig. 8, one can conclude the following: - (I) UV irradiation has mostly no action on phenol over the reaction time (4h). This result is in accordance with the previous report by Ghanem et al. [58]. (II) The percentage removal of phenol in presence of PAH and PABN in the first run was found ~ 84% and 90%, respectively, Fig. 8A. Moreover, at the beginning of the reaction, at 20 min., the rate of the

reaction was very high for both substances, i.e., PAH recorded 70% and PABN recorded 76% of phenol degradation. These results indicate the improvement of phenol removal after inclusion of biochar in the poly acrylamide matrix. It can be claimed that, the small increment in the phenol elimination percentage (6%) might be attributed to the low content of biochar nanorods in the polyacrylamide matrix. It is expected that, the complete demineralization of the phenolic water would be achieved by increasing of biochar content. (III) Nevertheless, the impact of the biochar was much significant in the second run. The removal of phenol was recorded 67 % and 87 % in the presence of PAH and PABN, respectively, Fig. 8B. This indicates that PAH lost ~ 20 % of its efficiency, meanwhile, PABN mostly maintained its activity. This observation was also recorded by Ghanem *et al.* [57]. In their study, the tested pristine polymer, which was also acted as a photocatalyst, lost its photocatalytic activity in the second run due to the consumption of its surface functional groups. (IV) In the dark, it was observed that, the percentage removal of phenol in presence of PAH and PABN was found ~ 85% and 65%, respectively. As clearly observed, PAH has almost the same removal percentages in the dark and even under UV irradiation. Even though, the rate of reaction was different, Fig 8 (A and C). Actually, the UV exposure assisted the removal process which might be attributed to the ability of PAH to absorb the UV wavelengths [59], which lie in the range of the used λ , and hence the probability to form reactive oxygen species (ROS) that responsible for phenol degradation. It is worth to mention that, PAH showed energy band gap of ~ 4.6 eV, Fig. 7B, which supports the hypothesis claimed that PAH can be used as a photocatalyst due to its ability to absorb the radiation. Then, the valance electrons can be excited from the valance band to the conduction band and hence the formation of ROS was acquired via adsorbed water and oxygen molecules. On the other hand, the pronounced decline in the phenol removal % by PABN might be attributed to the surface area (c.f. Fig. 6 and Table 1) as it was found that the incorporation of biochar nanorods in the PAH matrix decreases the S_{BET} .

Indeed, this result is not harmonious with Afjeh *et al.* findings [32]. In their research, they found that the inclusion of biochar in the PAH improved the removal of phenol. This might be attributed to the very low phenol concentration used in their study (50 mg/L) as well as the differences in the preparation and the reaction conditions. However, in our study, more than 10 folds of their concentration was used; (600 mg/L). As previously reported, increasing the initial concentration of phenol leads to decrease the removal efficiency by saturation of the adsorbent' active sites [60]. Therefore, the reaction rate was very high at the beginning of reaction at 20 min. and then slowly increased over the time due to the blocking of the hybrid hydrogel active sites. This might be revealed to the higher pore radius of PABN than of PAH sample, Table 1, which contributes in the adsorption process.

According to the previous discussions, it can be claimed that biochar nanorods has a synergistic effect in the PAH matrix. As shown, the phenol removal percentage increased in the presence of biochar in the both of first and second cycles, in particular, under the UV luminance. This indicates that the prepared biochar nanorods has a photocatalytic action. This might be attributed to the oxygenated functional groups on the surface of biochar that enhance the adsorption of oxygen molecules required to the photodegradation reaction. The same observation was recorded for graphene oxide and its reduced form by Ghanem *et al.* as the phenol degradation % was the highest in case of using graphene oxide whose surface rich of oxygen functional groups [52]. Basically, the amount of oxygen gas molecules adsorbed on the surface relies on the number of oxygen functional groups found on the surface [61]. Thus, the rate at the beginning of the degradation reaction was fast due to the presence of surface hydroxyl groups in biochar, as confirmed by FTIR in Fig. 2, that promote the adsorption of more oxygen molecules. Also, the photocatalytic degradation of phenol has been increased due to the enhancement of mass transfer.

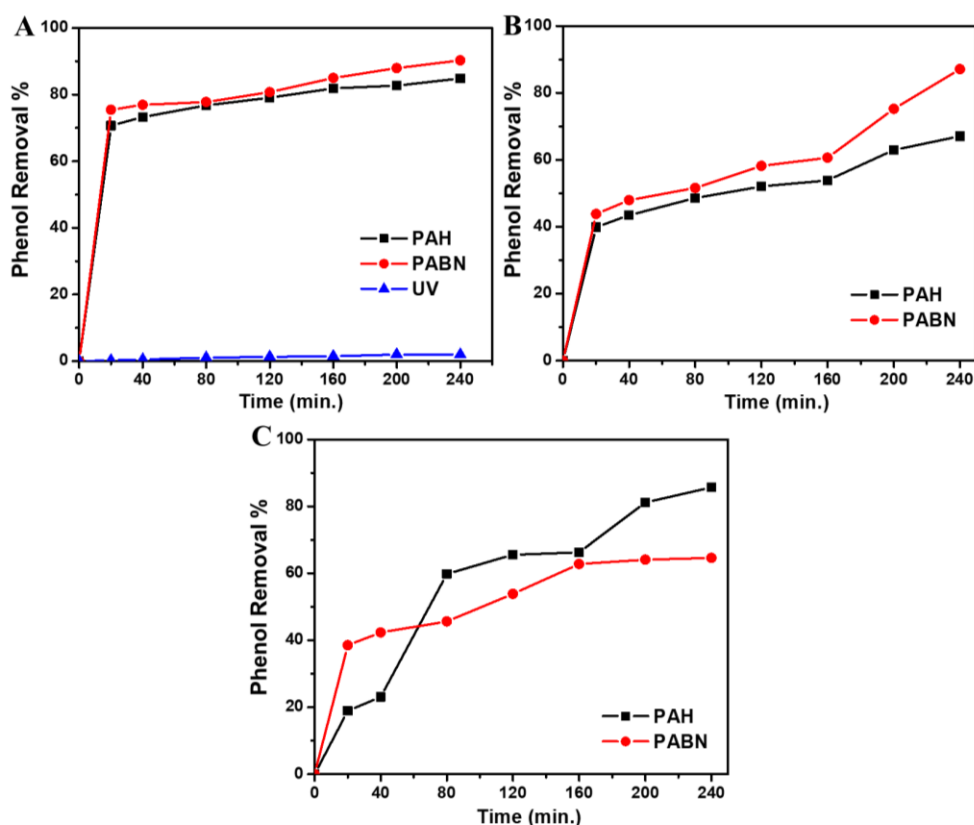


Figure 8: Phenol removal percentage under UV irradiation against the reaction time for polyacrylamide hydrogel (PAH) and its nanocomposite (PABN) after (A) first run and (B) second run. (C) Phenol removal percentage during adsorption in the dark using the same catalysts.

It is known that biochar is one of carbonaceous materials. Therefore, biochar could show high workability in photocatalytic degradation of phenol according to the published mechanism by Ghanem et al. [52]. Briefly, biochar, similar to exfoliated graphite, might absorb UV due to $\pi-\pi^*$ and $n-\pi^*$ energy levels [62]. Fascinatingly, Peng et al. studied the effect of UV irradiation on biochar. They recorded an increasing in the biochar surface area and huge amount of oxygen functional groups, such as carboxyl, lactonic, and hydroxyl, were formed on its surface upon UV exposure [63]. Furthermore, phenol can be adsorbed at the biochar surface due to $\pi-\pi$ interaction and hydrogen bonding [64]. This could contribute in the understanding of the high rate at the beginning of the reaction which might be attributed to the improvement of phenol adsorption. Moreover, the electrons can be also excited to the conduction band and interact with the dissolved oxygen to produce the superoxides [52]. Then, the created holes could oxidize the adsorbed pollutant molecules. On the other hand, the structure defects in biochar play a

crucial role in the degradation process as they act as highly reactive sites that could assist the phenol degradation [65, 66]. Also, resembles to graphene, the structural defects in biochar could create new energy levels which might contribute in the absorption of radiation and hence ROS formation [67]. Particularly, inclusion of biochar in PAH matrix increased the energy band gap by 1.8 eV, Fig. 7C. No doubt, this led to decrease the electron-hole recombination and hence improve the photocatalytic activity [57]. This might explain the performance of PABN particularly in the second run, unlike PAH. More details about introducing of biochar as an adsorbent, a catalyst, and a photocatalyst were previously reported [68]. Finally, in order to confirm the robustness and the efficiency of the prepared nanocomposite hydrogel, Table 2 showed a comparison with the previous work in the removing of phenol utilizing hydrogels, biochar, and their composites utilizing adsorption technique at different reaction conditions.

Table 2: Comparison between some of recent published adsorbents for phenols removal

Composite	Conditions	Phenol Removal	Ref.
<i>Polyacrylamide / rice husk biochar composite hydrogel</i>	Biochar content = 4.8 %, Catalyst weight = 50 mg/50mL, Temp. = 25 °C, pH=7, Time= 11 days, Phenol concn. = 50 mg/L, Technique: adsorption.	82.8 %	[32]
<i>Pectin / poly (acrylamide-co-2-acrylamido-2-methyl-1-propane sulfonic acid) hydrogel</i>	Catalyst weight = 0.5g/50mL, Temp. = 25 °C, pH = 3, Time= 240 min, Phenol concn. = 300 mg/L, Technique: adsorption.	87.3 %	[69]
<i>Polyacrylamide / starch hybrid hydrogel</i>	Catalyst weight = 200mg, Time= 24 hrs, Phenol concn. = 200 mg/L, Technique: adsorption	86.4 %	[19]
<i>Cross-linked polyacrylamide hydrogel</i>	Catalyst weight = 0.1g/ 25 mL, Temp. = 25 °C, pH = 4, Time= 24 hrs., Polyphenol concn. = 1 mg/mL, Technique: adsorption.	90.1 %	[70]
<i>Biochar produced from Araucaria Columnaris bark</i>	Catalyst weight = 0.5g/ 210 mL, Temp. = 25 °C, pH = 6, Time= 350 min, phenol concn. = 500 mg/L, Technique: adsorption.	41.9 mg/g	[71]
<i>Polyacrylamide / chicken biochar composite hydrogel</i>	Catalyst weight = 0.05 g/ 50 mL, Temp. = 25 °C, pH = 10, Time= 15 days, phenol concn. = 20 mg/L, Technique: adsorption.	21.83 mg/g	[31]
<i>Polyacrylamide / wood biochar composite hydrogel</i>	Catalyst weight = 0.05 g/ 50 mL, Temp. = 25 °C, pH = 10, Time= 15 days, phenol concn. = 20 mg/L, Technique: adsorption.	23.14 mg/g	[31]
<i>Polyacrylamide / tire biochar composite hydrogel</i>	Catalyst weight = 0.05 g/ 50 mL, Temp. = 25 °C, pH = 10, Time= 15 days, phenol concn. = 20 mg/L, Technique: adsorption.	14.04 mg/g	[31]
<i>Eucalyptus wood biochar</i>	Catalyst weight = 30 mg/ 50 mL, Temp. = 15 °C, pH = 7, Time= 4 hrs., phenol concn. = 100 mg/L, Technique: adsorption.	308 mg/g	[72]
<i>Biochar produced from Chinese herb residue</i>	Catalyst weight = 0.1 mg/ 20 mL, Temp. = 45 °C, pH = 7, Time= 360 min., phenol concn. = 50 mg/L, Technique: adsorption.	97 %	[73]
<i>Local biochar</i>	Catalyst weight = 0.5 mg/ 20 mL, Temp. = 25 °C, pH = 7, Time= 5 min., phenol concn. = 100 mg/L, Technique: adsorption.	55 %	[74]
<i>Polyacrylamide / palm kernal biochar composite hydrogel</i>	Catalyst weight = 0.1 g/ 100 mL, Temp. = 25 °C, pH = 6.8, Time= 2 days, phenol concn. = 10 mg/L, Technique: adsorption.	79 %	[30]
<i>Polyacrylamide / rice husk biochar composite hydrogel</i>	Catalyst weight = 1 g/ 500 mL, pH = 7, Time= 240 min., phenol concn. = 600 mg/L, Technique: photocatalysis.	91 %	This Study

3.7 Biological Activity

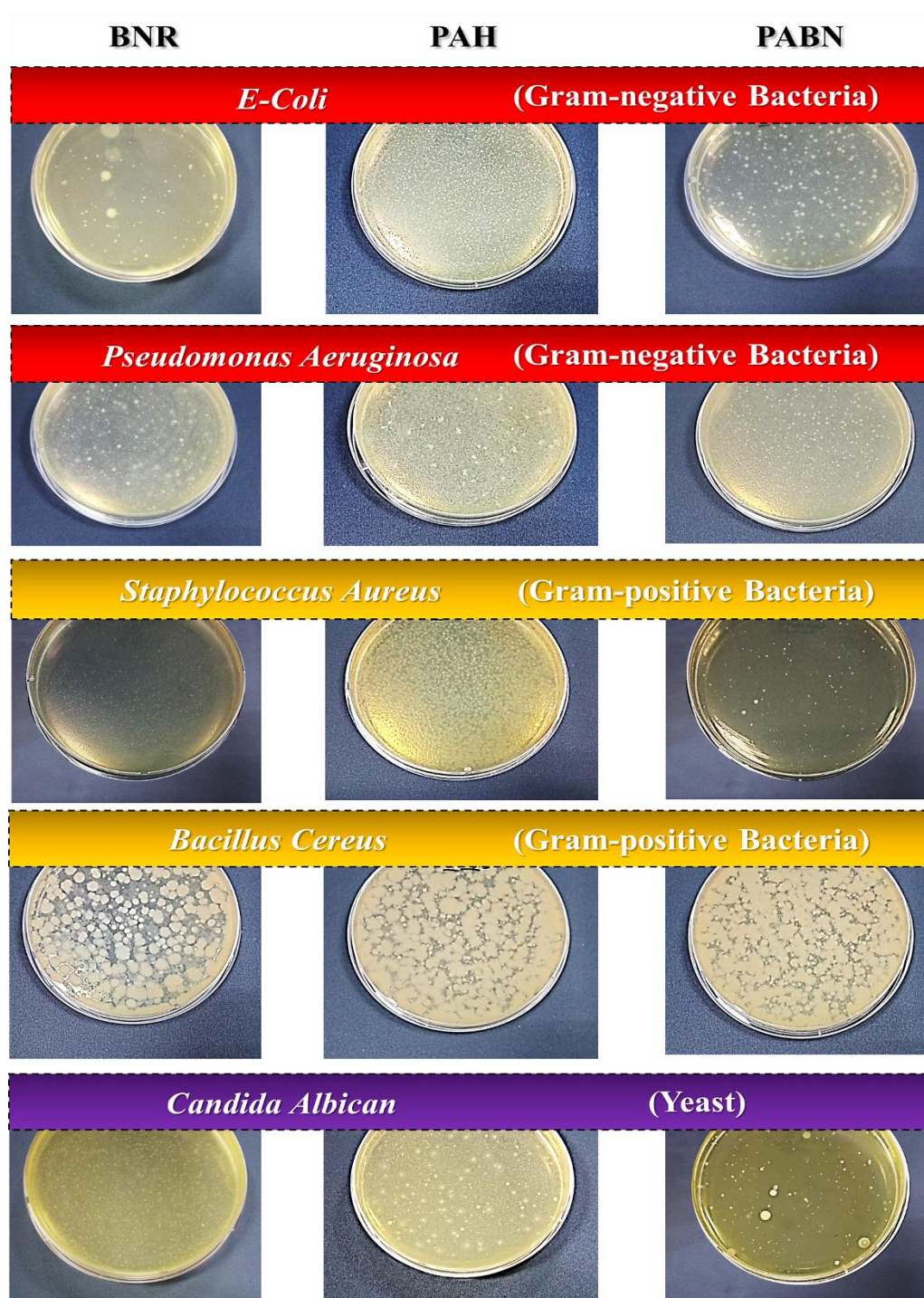


Figure 9: Colony forming unit of polyacrylamide hydrogel (PAH), Biochar (BNR), and their biochar nanocomposite (PABN).

The biocidal potential of the prepared materials was examined against five microorganisms as illustrated in Table 3. The results in this table represent the reduction % of the microbial growth in presence of tested samples i.e., the greater reduction %, the stronger antimicrobial agent is. Moreover, CFU was performed to confirm the results of OD, Fig. 9. In each agar plate, the number of microbial colonies indicates to the biocidal strength i.e., the lowest number of colonies forming units emphasizes. Nevertheless, carbonaceous materials cannot be equated with the metallic or metal oxide nanoparticles that have a strong activity [83].

Indeed, inclusion of BNR imparted PAH matrix a biological effect. Obviously, the microbial reduction against all the tested microorganisms increased compared with the pristine matrix, Table 3 and Fig. 9. However, the reduction of microbial growth still low which might be attributed to the very low biochar content (0.15 wt.%) in the polyacrylamide matrix. It is expected that the biological activity of the

the highest antimicrobial activity. Generally, PAH has mostly no antimicrobial performance as it showed a high microbial growth. BNR displayed the highest biological action against all tested microorganisms. However, *E-coli*, *Pseudomonas aeruginosa* and *Staphylococcus aureus* showed the lowest growth which emphasizes that the biochar has a strong ability against these microorganisms. Several researches discussed the biological performance of carbon nanomaterials including biochar [75-82]. nanocomposite hydrogel would be enhanced by increasing the biochar wt.% in the matrix. Particularly, biochar has a plenty of surface oxygenated function groups, as confirmed by FTIR in Fig. 2, that might responsible for the creation of the reactive oxygen species (ROS) as discussed in the previous section. These radicals cause an oxidative stress on the lipid bilayer of the microbial cell membranes leading to leakage of the cell' contents and death of the cell [75].

Table 3: Optical density reduction (OD %) of Gram-positive and Gram-negative bacteria, as well as yeast that are exposed to biochar (BNR), polyacrylamide hydrogel (PAH), and their nanocomposite (PABN).

Sample	Gram-positive Bacteria		Gram-negative Bacteria		Yeast
	<i>Escherichia coli</i>	<i>Pseudomonas aeruginosa</i>	<i>Bacillus cereus</i>	<i>Staphylococcus aureus</i>	<i>Candida albican</i>
BNR	61.33	58.66	42.39	59.99	42.64
PAH	12.93	6.67	6.97	16.66	Nil
PABN	20.71	22.29	19.53	24.98	32.52

4. Conclusions

Biochar nanorods were prepared using rice husk as precursor under carbonization conditions. Polyacrylamide hydrogel was obtained in water via polymerization of acrylamide monomer in presence of potassium per sulphate and N, N' methylene Bis acrylamide as an initiator and a crosslinker, respectively. Utilizing in-situ polymerization technique, biochar nanorods were incorporated in the polyacrylamide hydrogel.

Morphological studies with SEM and TEM confirmed the nanorods shape and size of the produced biochar in addition to their well dispersion in the hydrogel matrix. XRD provided a crystalline description for the prepared biochar nanorods. FTIR proved the strong hydrogen bonding within the nanocomposite matrix. Thermal analysis confirmed the improvement in the thermal stability of the prepared hybrid as the degradation temperature was shifted by ~ 40 degrees. Surface texture analysis displayed an enhancement in the average pore radius

and the average particle radius with a decline in the S_{BET} after inclusion of BNRs in PAH. The energy band gap of the produced hydrogel was increased by 1.8 eV in the presence of biochar nanorods which did not reflect any negative impact on the photocatalytic performance of the formed nanocomposite.

The demineralization of the phenolic synthetic wastewater emphasized the high performance of the nanocomposite hydrogel under UV irradiation. It recorded maximum phenol removal of 90% and 87 % in the first and the second cycle, respectively. Meanwhile, polyacrylamide showed a decay in the second run as it recorded maximum phenol removal of 67% compared to 84 % found in the first cycle. Moreover, the rate of the reaction was very high in particular at the beginning of process under the UV luminance compared with the rate in the dark which emphasized the impact of photocatalysis.

Also, the antimicrobial assessment for the prepared materials presented the biocidal potential of the obtained biochar nanorods against Gram-positive and Gram-negative bacteria as well as yeast. Inclusion of these nanorods in the polyacrylamide hydrogel enhanced its antimicrobial action.

Finally, it could be claimed that the polyacrylamide was imparted not only a photocatalytic activity but also an antimicrobial performance thanks to the presence of biochar nanorods. Without doubt, the prepared nanocomposite hydrogel can be used as a promising photocatalyst with a disinfecting ability.

8. References

1. Pardo, A.P., et al., *Modelling of an oil refinery wastewater treatment plant*. Environmental technology, 2007. **28**(11): p. 1273-1284.
2. Ioannou, Z. and J. Simitzis, *Adsorption kinetics of phenol and 3-nitrophenol from aqueous solutions on conventional and novel carbons*. Journal of Hazardous Materials, 2009. **171**(1-3): p. 954-964.
3. Adak, A., A. Pal, and M. Bandyopadhyay, *Removal of phenol from water environment by surfactant-modified alumina through adsolubilization*. Colloids and Surfaces A: Physicochemical and Engineering Aspects, 2006. **277**(1-3): p. 63-68.
4. Xu, Y., et al., *Research status, industrial application demand and prospects of phenolic resin*. RSC advances, 2019. **9**(50): p. 28924-28935.
5. Caturla, F., et al., *Adsorption of substituted phenols on activated carbon*. Journal of colloid and interface science, 1988. **124**(2): p. 528-534.
6. Michałowicz, J. and W. Duda, *Phenols--Sources and Toxicity*. Polish Journal of Environmental Studies, 2007. **16**(3).
7. Nabais, J.V., et al., *Phenol removal onto novel activated carbons made from lignocellulosic precursors: influence of surface properties*. Journal of hazardous materials, 2009. **167**(1-3): p. 904-910.
8. de Sousa Ribeiro, L.A., et al., *Preparation, characterization, and application of low-cost açai seed-based activated carbon for phenol adsorption*. International Journal of Environmental Research, 2018. **12**: p. 755-764.
9. Juang, R.-S., H.-C. Kao, and K.-J. Tseng, *Kinetics of phenol removal from saline solutions by solvent extraction coupled with degradation in a two-phase partitioning bioreactor*. Separation and purification technology, 2010. **71**(3): p. 285-292.
10. Thepsithar, P. and E.P. Roberts, *Removal of phenol from contaminated kaolin using electrokinetically enhanced in situ chemical*

5. Conflicts of interest

Authors declare there is no conflict of interest.

6. Formatting of funding sources

This work was supported by self-funding

7. Acknowledgment

The authors are grateful for Mansoura University and National Research Centre for providing the workplace and the required facilities in order to achieve the research objectives.

oxidation. Environmental science & technology, 2006. **40**(19): p. 6098-6103.

11. Busca, G., et al., *Technologies for the removal of phenol from fluid streams: a short review of recent developments*. Journal of hazardous materials, 2008. **160**(2-3): p. 265-288.

12. Pradeep, N., et al., *Biological removal of phenol from wastewaters: a mini review*. Applied Water Science, 2015. **5**: p. 105-112.

13. Crini, G. and E. Lichtfouse, *Advantages and disadvantages of techniques used for wastewater treatment*. Environmental Chemistry Letters, 2019. **17**: p. 145-155.

14. Mohamed, A., et al., *Rapid photocatalytic degradation of phenol from water using composite nanofibers under UV*. Environmental Sciences Europe, 2020. **32**: p. 1-8.

15. Ahmed, E.M., et al., *An innovative method for preparation of nanometal hydroxide superabsorbent hydrogel*. Carbohydrate polymers, 2013. **91**(2): p. 693-698.

16. Shah, L.A. and S.A. Khan, *Polymer hydrogels for wastewater treatment*, in *Environmental chemistry and recent pollution control approaches*. 2019, IntechOpen.

17. Nakhjiri, M.T., G.B. Marandi, and M. Kurdtabar, *Poly (AA-co-VPA) hydrogel cross-linked with N-maleyl chitosan as dye adsorbent: Isotherms, kinetics and thermodynamic investigation*. International Journal of Biological Macromolecules, 2018. **117**: p. 152-166.

18. Guo, M., et al., *Cellulose-based thermosensitive supramolecular hydrogel for phenol removal from polluted water*. Environmental Research, 2022. **214**: p. 113863.

19. Dutra, M.A.L., et al., *Phenol removal from wastewater using eco-friendly hybrid hydrogels*. Journal of Applied Polymer Science, 2021. **138**(30): p. 50725.

20. Badawy, A.A., et al., *Utilization and characterization of cellulose nanocrystals decorated with silver and zinc oxide nanoparticles for removal of lead ion from wastewater*. Environmental Nanotechnology, Monitoring & Management, 2021. **16**: p. 100501.
21. Marandi, G.B., Z.P. Kermani, and M. Kurdtabar, *Fast and efficient removal of cationic dyes from aqueous solution by collagen-based hydrogel nanocomposites*. Polymer-Plastics Technology and Engineering, 2013. **52**(3): p. 310-318.
22. Wang, J., et al., *Adsorptive removal of phenol by single and double network composite hydrogels based on hydroxypropyl cellulose and graphene oxide*. Journal of Materials Research, 2018. **33**(23): p. 3898-3905.
23. Ibrahim, S.M., et al., *Effective single and contest carcinogenic dyes adsorption onto A-zeolite/bacterial cellulose composite membrane: Adsorption isotherms, kinetics, and thermodynamics*. Journal of Environmental Chemical Engineering, 2022. **10**(6): p. 108588.
24. Oleszczuk, P., et al., *Characterization of nanoparticles of biochars from different biomass*. Journal of Analytical and Applied Pyrolysis, 2016. **121**: p. 165-172.
25. Weber, K. and P. Quicker, *Properties of biochar*. Fuel, 2018. **217**: p. 240-261.
26. Tomczyk, A., Z. Sokołowska, and P. Boguta, *Biochar physicochemical properties: pyrolysis temperature and feedstock kind effects*. Reviews in Environmental Science and Bio/Technology, 2020. **19**: p. 191-215.
27. Xiang, W., et al., *Biochar technology in wastewater treatment: A critical review*. Chemosphere, 2020. **252**: p. 126539.
28. Sanyang, M., et al., *Hydrogel biochar composite for arsenic removal from wastewater*. Desalination and Water Treatment, 2016. **57**(8): p. 3674-3688.
29. Sanyang, L., et al., *Zinc removal from wastewater using hydrogel modified biochar*. Applied Mechanics and Materials, 2014. **625**: p. 842-846.
30. Sanyang, L., W. Ghani, and R. Zainudin, *Sorption of Phenol from Wastewater by Hydrogel-biochar Composite*. International Journal of Engineering and Technology, 2013. **10**(1): p. 38-49.
31. Karakoyun, N., et al., *Hydrogel-Biochar composites for effective organic contaminant removal from aqueous media*. Desalination, 2011. **280**(1-3): p. 319-325.
32. Sadeghi Afjeh, M., G. Bageri Marandi, and M.J. Zohuriaan-Mehr, *Hydrogel-rice husk biochar composite as an adsorbent for the removal of phenol and PNP from aqueous solutions*. Separation Science and Technology, 2021. **56**(7): p. 1195-1210.
33. Abdullahi, S.S., et al., *Simple method for the determination of band gap of a nanopowdered sample using Kubelka Munk theory*. NAMP J, 2016. **35**: p. 241-246.
34. Ghanem, A.F., et al., *Investigation of water sorption, gas barrier and antimicrobial properties of polycaprolactone films contain modified graphene*. Journal of Materials Science, 2021. **56**: p. 497-512.
35. Krishnasamy, S., et al., *Decolourization of Reactive Red 120 using agro waste-derived biochar*. Advances in Materials Science and Engineering, 2022. **2022**.
36. Mohan, D., et al., *Biochar production and applications in soil fertility and carbon sequestration—a sustainable solution to crop-residue burning in India*. RSC advances, 2018. **8**(1): p. 508-520.
37. Kim, S., et al., *Polyacrylamide hydrogel properties for horticultural applications*. International Journal of Polymer Analysis and Characterization, 2010. **15**(5): p. 307-318.
38. Šimon, E.K.-P.Š.-P. and A. GATIAL, *Confirmation of polymerisation effects of sodium chloride and its additives on acrylamide by infrared spectrometry*. Journal of Food and Nutrition Research, 2007. **46**(1): p. 39-44.
39. Ganesan, A., et al., *Nanoporous rice husk derived carbon for gas storage and high performance electrochemical energy storage*. Journal of Porous Materials, 2014. **21**: p. 839-847.
40. Zhang, S. and J. Wang, *Removal of chlortetracycline from water by immobilized Bacillus subtilis on honeysuckle residue-derived biochar*. Water, Air, & Soil Pollution, 2021. **232**(6): p. 236.
41. Mora, A.-S., et al., *A perspective approach on the amine reactivity and the hydrogen bonds effect on epoxy-amine systems*. European Polymer Journal, 2020. **123**: p. 109460.
42. Avorny, V.K., et al., *Temperature effects on properties of rice husk biochar and calcinated Burkina phosphate rock*. Agriculture, 2021. **11**(5): p. 432.
43. Sarkar, S. and S.K. Das, *Removal of Cr (VI) and Cu (II) ions from aqueous solution by rice husk ash—column studies*. Desalination and Water Treatment, 2016. **57**(43): p. 20340-20349.
44. Ibrahim, A.G., et al., *Synthesis of poly (acrylamide-graft-chitosan) hydrogel: Optimization of the grafting parameters and swelling studies*. Am. J. Polym. Sci. Technol, 2019. **5**: p. 55-62.
45. Zanjani, J.S.M., et al., *Rational design and direct fabrication of multi-walled hollow electrospun fibers with controllable structure and surface properties*. European Polymer Journal, 2015. **62**: p. 66-76.
46. Das, C., et al., *Incorporation of biochar to improve mechanical, thermal and electrical*

- properties of polymer composites*. Polymers, 2021. **13**(16): p. 2663.
47. Tsai, C.-Y., et al., *Engineered mesoporous biochar derived from rice husk for efficient removal of malachite green from wastewaters*. Bioresource Technology, 2022. **347**: p. 126749.
48. Evingür, G.A. and Ö. Pekcan, *Optical energy band gap of PAAm-GO composites*. Composite Structures, 2018. **183**: p. 212-215.
49. Chen, W.-C., et al., *Theoretical and experimental characterization of small band gap poly (3, 4-ethylenedioxythiophene methine) s*. Macromolecules, 2004. **37**(16): p. 5959-5964.
50. Rawat, A., et al., *Optical band gap of Polyvinylpyrrolidone/Polyacrylamide blend thin films*. Indian Journal of Pure and Applied Physics, 2012. **50**: p. 100-104.
51. Velo-Gala, I., et al., *Role of activated carbon on micropollutants degradation by ionizing radiation*. Carbon, 2014. **67**: p. 288-299.
52. Ghanem, A.F., et al., *Synergistic effect of zinc oxide nanorods on the photocatalytic performance and the biological activity of graphene nano sheets*. Heliyon, 2020. **6**(2): p. e03283.
53. Meng, L., et al., *Photocatalytic behavior of biochar-modified carbon nitride with enriched visible-light reactivity*. Chemosphere, 2020. **239**: p. 124713.
54. Singaravelan, R. and S. Bangaru Sudarsan Alwar, *Electrochemical synthesis, characterisation and phytogenic properties of silver nanoparticles*. Applied Nanoscience, 2015. **5**: p. 983-991.
55. Gabhi, R.S., D.W. Kirk, and C.Q. Jia, *Preliminary investigation of electrical conductivity of monolithic biochar*. Carbon, 2017. **116**: p. 435-442.
56. Bartoli, M., et al., *Effect of heating rate and feedstock nature on electrical conductivity of biochar and biochar-based composites*. Applications in Energy and Combustion Science, 2022. **12**: p. 100089.
57. Ghanem, A.F., et al., *Enhancement the photocatalytic and biological activity of nano-sized ZnO using hyperbranched polyester*. Journal of Inorganic and Organometallic Polymers and Materials, 2019. **29**: p. 928-938.
58. Ghanem, A., et al., *Photocatalytic activity of hyperbranched polyester/TiO₂ nanocomposites*. Applied Catalysis A: General, 2014. **472**: p. 191-197.
59. Verma, A., et al., *The functionalization of polyacrylamide with MoS₂ nanoflakes for use in transient photodetectors*. Sustainable Energy & Fuels, 2021. **5**(5): p. 1394-1405.
60. Al-Ghouti, M.A., et al., *Effective removal of phenol from wastewater using a hybrid process of graphene oxide adsorption and UV-irradiation*. Environmental Technology & Innovation, 2022. **27**: p. 102525.
61. Groeneveld, I., et al., *Parameters that affect the photodegradation of dyes and pigments in solution and on substrate—An overview*. Dyes and Pigments, 2022: p. 110999.
62. Uran, S., A. Alhani, and C. Silva, *Study of ultraviolet-visible light absorbance of exfoliated graphite forms*. AIP Advances, 2017. **7**(3).
63. Peng, Z., et al., *UV modification of biochar for enhanced hexavalent chromium removal from aqueous solution*. Environmental Science and Pollution Research, 2018. **25**: p. 10808-10819.
64. Thang, P.Q., et al., *Potential application of chicken manure biochar towards toxic phenol and 2, 4-dinitrophenol in wastewaters*. Journal of environmental management, 2019. **251**: p. 109556.
65. Li, H., et al., *Persulfate adsorption and activation by carbon structure defects provided new insights into ofloxacin degradation by biochar*. Science of The Total Environment, 2022. **806**: p. 150968.
66. Ouyang, D., et al., *Activation mechanism of peroxymonosulfate by biochar for catalytic degradation of 1, 4-dioxane: Important role of biochar defect structures*. Chemical Engineering Journal, 2019. **370**: p. 614-624.
67. Nag, A., J. Kumar, and O. Sastri. *Electronic properties of graphene and effect of doping on the same*. in *AIP Conference Proceedings*. 2015. AIP Publishing.
68. Gasim, M.F., et al., *Application of biochar as functional material for remediation of organic pollutants in water: an overview*. Catalysts, 2022. **12**(2): p. 210.
69. Kumar, C.R., et al., *Selective Adsorption of Phenol and Resorcinol from Aqueous Solution by Pectin/Poly (Acrylamide-Co-2-Acrylamido-2-Methyl-1-Propanesulfonic Acid) Chelating (PPAA) Hydrogels: Equilibrium, Kinetics, and Modeling*. Journal of Innovative Technology, 2021. **3**(1): p. 47-55.
70. Cao, Y., X. Qi, and H. Yan, *Selective adsorption of tannins over small polyphenols on cross-linked polyacrylamide hydrogel beads and their regeneration with hot water*. Reactive and Functional Polymers, 2020. **146**: p. 104398.
71. Chandola, D., P. Thathola, and A. Bisht, *Removal of phenol from aqueous solution using biochar produced from Araucaria Columnaris Bark*. 2021.
72. Singh, R., et al., *High surface area Eucalyptus wood biochar for the removal of phenol from petroleum refinery wastewater*. Environmental Challenges, 2021. **5**: p. 100353.
73. Zhang, Y., et al. *Study on adsorption of phenol from aqueous media using biochar of Chinese herb residue*. in *IOP Conference Series: Materials Science and Engineering*. 2018. IOP Publishing.

74. Elbidi, M., et al., *Comparative Study between Activated Carbon and Biochar for Phenol Removal from Aqueous Solution*. BioResources, 2021. **16**(4).
75. Ghanem, A.F., et al., *Synergistic effect of zinc oxide nanorods on the photocatalytic performance and the biological activity of graphene nano sheets*. Heliyon, 2020. **6**(2).
76. Hasanuzzaman, M., et al., *Biochar and chitosan regulate antioxidant defense and methylglyoxal detoxification systems and enhance salt tolerance in jute (Corchorus olitorius L.)*. Antioxidants **10**, 2017. 2021.
77. Valenca, R., et al., *Biochar role in improving pathogens removal capacity of stormwater biofilters, in Advances in Chemical Pollution, Environmental Management and Protection*. 2021, Elsevier. p. 175-201.
78. Wang, Z., et al., *Effects of biochar carried microbial agent on compost quality, greenhouse gas emission and bacterial community during sheep manure composting*. Biochar, 2023. **5**(1): p. 3.
79. Gurtler, J.B., et al., *Biocidal activity of fast pyrolysis biochar against escherichia coli O157: H7 in soil varies based on production temperature or age of biochar*. Journal of Food Protection, 2020. **83**(6): p. 1020-1029.
80. Mohanty, S.K., et al., *Efficacy of biochar to remove Escherichia coli from stormwater under steady and intermittent flow*. Water research, 2014. **61**: p. 288-296.
81. Dizaj, S.M., et al., *Antimicrobial activity of carbon-based nanoparticles*. Advanced pharmaceutical bulletin, 2015. **5**(1): p. 19.
82. Giraud, L., A. Tourrette, and E. Flahaut, *Carbon nanomaterials-based polymer-matrix nanocomposites for antimicrobial applications: A review*. Carbon, 2021. **182**: p. 463-483.
83. El-Gendi, A., et al., *Antifouling and antimicrobial polyethersulfone/hyperbranched polyester-amide/Ag composite*. RSC advances, 2020. **10**(41): p. 24169-24175.